



Study on the mechanism of quasi-continuous wave (QCW) fiber laser low-damage processing of carbon fiber-reinforced plastics

Liao Zhou¹ · Jia Zhou¹ · Ping Huang¹ · Guanghui Zhang¹ · Ze Lin¹ · Zhen Zhao¹ · Yuxing Huang¹ · Hui Jiao¹ · Yuhong Long¹

Received: 6 June 2022 / Accepted: 24 October 2022 / Published online: 23 November 2022
© The Author(s), under exclusive licence to Springer-Verlag London Ltd., part of Springer Nature 2022

Abstract

To explore the method of laser low-damage processing of carbon fiber-reinforced plastics (CFRP). The feasibility of reducing the thermal damage of CFRP by laser processing with a 450 W QCW fiber laser through a multi-pass strategy was investigated by the design of experiments (DOE) in this paper. The mechanism of material removal and heat-affected zone (HAZ) formation of laser processing CFRP were elucidated by experimental study and finite element analysis. The results show that HAZ formation can be effectively controlled by the pulsed mode with a multi-pass strategy (up to 7 cuts) and high cutting speed (up to 200 mm/s), with the minimum surface HAZ 19.5 μm . The low-power multi-pass strategy is conducive to the effective cooling of the internal kerf by the auxiliary gas, which avoids the thermal damage of the material caused by excessive heat accumulation, and the processing quality is improved. The finite element model shows that the temperature field distribution range is smaller when the laser is parallel to the axis of the carbon fiber, and a smaller HAZ and a larger groove width can be obtained. The HAZ will be formed when the removal of resin and carbon fiber is inconsistent. Finally, the statistics analyze the influence of process parameters on machining quality, and the process parameters are optimized and matched. This study provides a reference for low-damage laser processing of CFRP.

Keywords QCW fiber laser · CFRP · Multi-pass strategy · Temperature field · HAZ

1 Introduction

Carbon fiber-reinforced plastics (CFRP) are a new composite material with excellent mechanical properties. CFRP has high strength, high specific heat capacity, low density, and good wear resistance [1–3]. It has been widely used in many industrial applications, such as aerospace, defense, medical, and automotive industries [4]. CFRP often cannot meet the assembly requirements and requires secondary processing, such as cutting and punching. There are several challenges to

cutting CFRP due to their anisotropy and excellent mechanical properties. Traditional machining has the defects of severe tool wear [5, 6], material delamination [7, 8], and high cost [9], which hinder the further application of CFRP. In non-traditional machining, electrical discharge machining has low efficiency [10, 11], and abrasive water jet machining [12–14] will cause defects such as high surface roughness and material delamination. However, laser machining has the advantages of no tool wear, small kerf, high machining accuracy, high efficiency, and low cost, and it is widely used in material processing. Laser processing mainly realizes material removal by thermal effect. Unfortunately, thermal damage is inevitable during processing. Some thermal defects [15–18] will be generated during CFRP laser processing due to the anisotropy of CFRP, such as heat-affected zone, taper angle, and fiber terminal expansion.

To explore the methods of reducing thermal damage during laser processing CFRP, this paper summarizes the research progress of laser processing CFRP at home and abroad. There are mainly two aspects to effectively controlling thermal damage. On the one hand, the auxiliary

✉ Yuxing Huang
1758655987@qq.com

✉ Hui Jiao
1020116567@qq.com

✉ Yuhong Long
longyuhong@guet.edu.cn

¹ School of Mechanical & Electrical Engineering, Guangxi Key Laboratory of Manufacturing Systems and Advanced Manufacturing Technology, Guilin University of Electronic Technology, Guilin 541004, Guangxi, China

cooling device is added during the laser processing process to reduce the residual heat of processing. Tangwarodomnukun et al. [19] used a 30 W nanosecond pulsed fiber laser with a wavelength of 1064 nm to process CFRP with a thickness of 3 mm under a flowing water layer. The results showed that HAZ could be effectively reduced, and fiber terminal expansion could be improved through the flowing water layer. Kaakkunen et al. [20] researched jetted thin water layer-assisted femtosecond laser processing of silicon wafers. The results showed that the sprayed thin water layer could drive the processing debris away from the processing area, which improved the machining quality. Sun et al. [21, 22] studied the effect of water jet-guided laser technology on the machining quality of CFRP. They found that the water-jet-guided laser technology could quickly cool the inside of the kerf, and the HAZ was effectively reduced. Simultaneously, the cleanliness of the kerf could be improved by the impact of the water jet on the kerf [23, 24]. However, the structure of the device is complex. The water has a better cooling effect; however, water will absorb the laser energy and cause problems such as laser scattering, leading to a large loss of laser energy and reducing processing efficiency [22]. Most importantly, CFRP easily absorbs moisture during processing, which decreases mechanical properties [25].

Studies have shown that gas-assisted lasers can avoid excessive loss of laser energy, which improves processing efficiency and obtains higher processing quality [26]. Sato et al. [27] conducted experiments on CFRP using high-power pulsed fiber lasers. N₂ and air assist on process quality were investigated, respectively. The results showed that HAZ could be effectively suppressed with N₂ assistance, and the cutting speed was increased by up to 10%. Negarestani et al. [28] used a nano-second pulsed diode-pumped solid-state Nd:YAG with a wavelength of 1064 nm to cut CFRP with a thickness of 1.2 mm. It was found that mixing a small amount of oxygen in the inert gas could reduce fiber pull-out by up to 55% and have higher processing efficiency. However, oxygen only significantly affects the deep layers [29]. Unfortunately, when the cutting depth is deep, the cooling effect of the gas is limited due to the transport factor, and a larger HAZ will be produced.

On the other hand, shortening the interaction time between the laser and the material can avoid more material damage caused by heat accumulation. A pulsed laser can reduce the contact time between the laser and the material [30]. Schneider et al. [31] compared the effect of continuous and pulsed lasers on the machining quality. They found that pulsed laser processing could achieve better machining quality at 100 m/min speeds. Li et al. [32] studied the hole quality of CFRP processed by fiber laser in continuous and pulsed modes, respectively. At the same time, the process parameters were optimized by statistics, which once again proved that the machining quality obtained was better with

the pulsed laser. The shorter the pulse width, the better the processing quality. However, the output power of ultra-short pulse width lasers is low, resulting in low processing efficiency [29].

Similarly, the interaction time between the laser and the material can be shortened by increasing the processing speed. Herzog et al. [33] used a 30KW CW fiber laser to cut CFRP with a thickness of 1.4 mm by single-pass and multi-pass scanning techniques. The experimental results showed that the single-pass cutting speed was as high as 1.2 m/s, and the HAZ was expanded to 139 μm . While the multi-pass cutting times were 16 times, the equivalent speed was 1.63 m/s, and the HAZ was reduced to 78 μm . C. Leone et al. [17] used a 150 W Nd:YAG pulsed laser to cut CFRP with a thickness of 1 mm at 10.8 mm/s, and the minimum HAZ was 170 μm . Li et al. [16] used a CW fiber laser to process CFRP. The smallest HAZ was obtained when the power was 650 W and the cutting speed was 1100 mm/min. When the multi-scan technique was used, processing efficiency was improved, and HAZ was also reduced, but the level of improvement of the HAZ was limited. This may be because the CW laser has no pulse-off time and relatively low cutting speed, resulting in a limited cooling effect, so there is still a large HAZ. Considering the analysis of the aforementioned works, there is a possibility for reducing HAZ through higher-power pulsed laser and high-speed processing.

With the continuous development of laser sources, the emergence of QCW fiber lasers provides new opportunities for the low-damage processing of CFRP. QCW fiber lasers can operate in both pulsed wave (PW) and continuous wave (CW) modes, and the peak power in pulsed mode is ten times higher than the average power. QCW fiber lasers can generate several kilowatts of peak power at low frequencies. Therefore, QCW lasers are very suitable for commercial processing. However, the current research on QCW fiber laser cutting of CFRP is limited. There are few reports on using the pulsed mode of QCW lasers at high cutting speed and power for multi-pass strategies to study the methods and mechanisms for reducing thermal damage.

This work aims to study the material removal mechanism and effect of laser process parameters (laser power, laser frequency, cutting speed, and pulse width) on the processing of a 450 W QCW fiber laser to process CFRP laminates with a thickness of 1 mm. According to the DOE, the orthogonal experiment L16(4⁴) was carried out, and the process parameters were optimized. The influence of process parameters on machining quality is analyzed statistically. The regression model between process parameters and machining quality is established. The effects of machining direction and cutting times on machining quality were compared. The mechanism of material removal and HAZ formation were analyzed by combining the experimental study and the finite element model (FEM). Finally, a method for controlling thermal

damage during QCW laser processing of CFRP is obtained. This study provides a reference for low-damage laser processing of CFRP.

2 Workpiece material, experimental facility, and experiment strategy

2.1 Workpiece material

Cutting tests were performed on a CFRP laminate with a thickness of 1 mm. The unidirectional laminate with the lamination structure of 0°/90° is composed of carbon fiber and an epoxy resin matrix. The schematic diagram of the structure is shown in Fig. 1. The single-layer thickness of CFRP is about 0.15 mm, and there are seven layers in total. The material physical parameters of CFRP are shown in Table 1.

2.2 Experiment facility

The QCW fiber laser cutting head used in this paper is shown in Fig. 2, the QCW fiber laser welding/cutting integrated machine (WCM-IQCW450) produced by Wuhan Rongke Laser Automation Co., Ltd. The laser adopts IPG quasi-continuous wave fiber laser (model: YLM-450_4500-QCW). The peak power of the pulsed mode is

several times that of the continuous mode. The energy is stable, and the photoelectric conversion efficiency is high. The basic parameters of QCW fiber laser are shown in Table 2, which can work in continuous and pulsed modes. The CFRP is clamped by the gripper and fixed to the stage surface on the mobile platform. In this paper, N₂ is used to assist the laser processing of CFRP with a gas pressure of 0.5Mpa. The gas is coaxial with the laser. The main function of N₂ is to enhance the cooling effect of the machining area. The laser focus was focused on the upper surface of CFRP, and the distance between the bottom of the laser nozzle and the surface of CFRP was 0.9 mm.

a is the peak power of pulsed mode; b is the average power of continuous mode.

The high-speed camera PCO. dimax HD was used to capture the in situ dynamic processes of laser processing CFRP from the side, with an exposure time of 900us and a rate of 1000 frames per second. The OLYMPUS LEXT OLS4100 3D laser measuring microscope produced by Olympus is used to capture the topography of the workpiece. The software associated with the microscope can display the specific data of the measurement position. Sandpaper with different roughness (P800, P1200, P2000) was used to polish the CFRP section. At the same time, the CFRP was cleaned by ultrasonic vibration in ethanol solution for 2 min, and the cross-sectional data was measured.

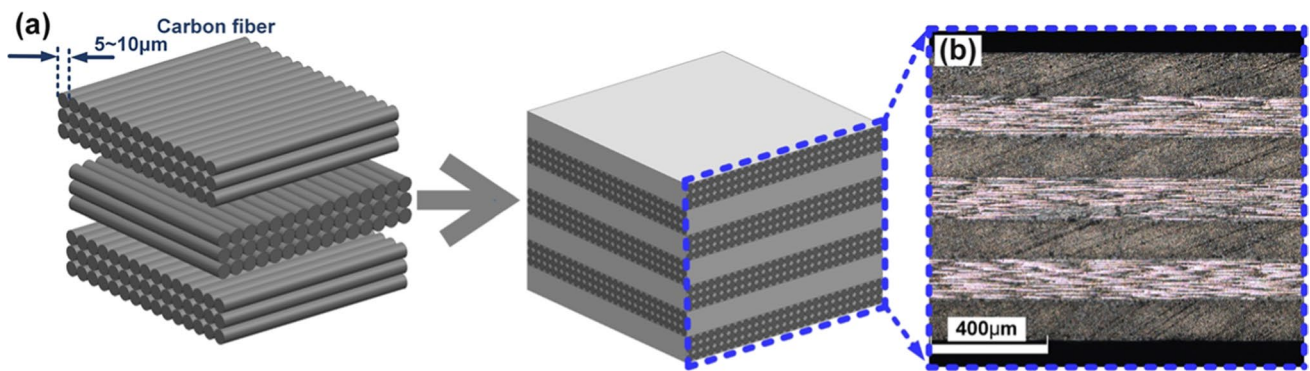


Fig. 1 The structure of CFRP. a The schematic diagram of CFRP structure. b The cross-section of CFRP

Table 1 Physical properties of CFRP

Index	Epoxy resin	Carbon fiber	Units
Density	1200	1850	kg/m ³
Thermal conductivity	0.1	50 (along fibers) 5 (perpendicular fibers)	W/(m*K)
Specific heat capacity	1884	710	J/(kg*K)
Vaporization temperature	698	3900	K
Latent heat	1000	43,000	kJ/kg
Volume fraction	30%	70%	—

Fig. 2 The diagram of laser processing. **a** The laser cutting head. **b** The schematic diagram of QCW fiber laser processing of QCW fiber laser processing CFRP

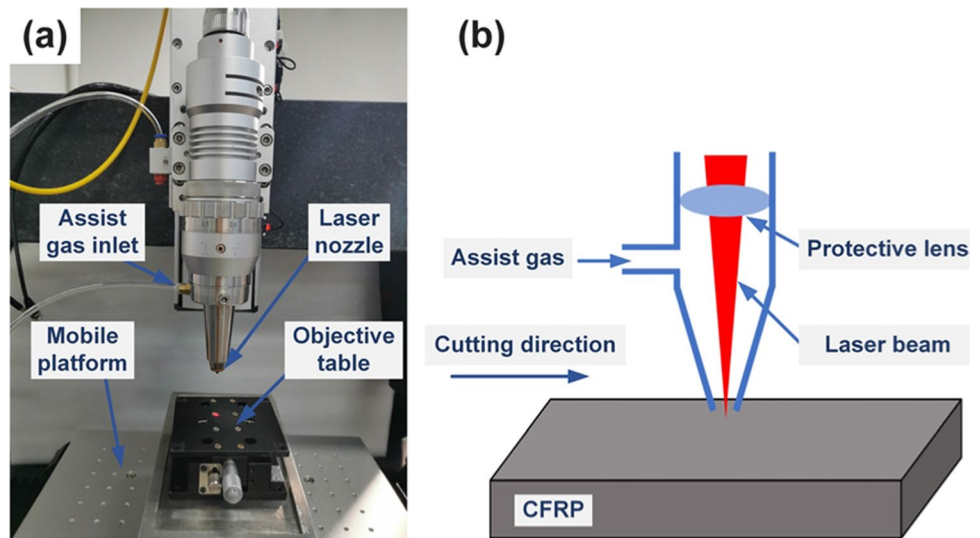


Table 2 Characteristics of QCW fiber laser system

Characteristics	Symbols	Values	Units
Wavelength	λ	1064	nm
Peak laser power ^a	P_{max}	4500	W
Nominal average power ^b	P_a	450	W
Pulse width	τ	0.1–50	ms
Single pulse energy	E	≤45	J
Focused spot radius	r_b	50	μm
Pulse frequency	f	0–2000	Hz
Scanning speed	V	0–200	mm/s
Mode of operation	—	CW/PW	—
Beam parameter product	BPP	2–3	mm × rad
Power consumption	—	2.5	kW

2.3 Experiment strategy

This study investigated the effect of QCW fiber laser multi-pass cutting at high speed on CFRP’s machining quality. The method of laser low-damage processing of CFRP was explored. The peak power can be adjusted by changing the laser power share (adjustable range 15–100%). Each groove is based on forming a continuous slit on the bottom surface of CFRP. No pause time is set between each cutting. Each process parameter in this experiment will be repeated four times to reduce the experimental error. Through the preliminary single-factor experimental exploration, it has been shown that the laser power (18–30%), laser frequency (1100–1400 Hz), cutting speed (140–200 mm/s), and laser pulse width (0.1–0.25 ms) can obtain better performance machining quality. When the laser share is 18%, 22%, 26%, and 30%, the corresponding laser power is 810 W, 990 W, 1170 W, and 1350 W, respectively, as shown in Table 3. Therefore, four factors

Table 3 Factors and adopted values for the orthogonal test

Factors	Values			
	Level 1	Level 2	Level 3	Level 4
Peak laser power (W)	810	990	1170	1350
Laser frequency (Hz)	1100	1200	1300	1400
Cutting speed (mm/s)	140	160	180	200
Pulse width (ms)	0.1	0.15	0.2	0.25

The bold entries are the optimized process parameters. The laser parameters used in the finite element model are the parameters in bold

Table 4 The symbol of each factor

Factors	Symbol	Factors	Symbol
Laser power	P_{max}	Surface HAZ	HAZ_S
Laser frequency	f	Groove width	G_w
Cutting speed	V	Cross section HAZ	HAZ_C
Pulse width	τ	Cutting times	C_t
		Depth heat width ratio	D_h_w

and four levels of orthogonal experiments were carried out for the above process parameters. The symbol of each factor is shown in Table 4, and the orthogonal experiment’s experimental results are shown in Table 5.

In this paper, factors that significantly affect the mechanical properties, such as surface HAZ, groove width, and section HAZ, are selected as the evaluation indicators of machining quality. The specific definitions are shown in Fig. 3. It is worth noting that the cross-section HAZ refers to the maximum HAZ value of the cross-section in this paper. At the same time, this paper uses the cutting times as one of the results because the cutting times can reflect the depth of a single cut. The more cutting times,

Table 5 The experimental results of orthogonal experiment

Experimental serial number	P_{\max}	f	V	τ	HAZ_S (μm)	G_w (μm)	HAZ_C (μm)	D_h_w (1/ μm)	C_t (-)
1	810	1100	140	0.10	19.500	109.000	114.250	0.080300323	6
2	810	1200	160	0.15	17.000	152.000	176.250	0.037327361	3
3	810	1300	180	0.20	27.125	173.250	218.500	0.026416502	3
4	810	1400	200	0.25	30.875	191.500	224.125	0.023299195	2
5	990	1100	160	0.20	34.375	173.750	175.250	0.032841060	2
6	990	1200	140	0.25	45.000	221.250	252.000	0.017935611	2
7	990	1300	200	0.10	21.000	147.500	140.500	0.048253815	5
8	990	1400	180	0.15	26.000	183.000	221.875	0.024628646	3
9	1170	1100	180	0.25	44.500	208.000	213.250	0.022544864	2
10	1170	1200	200	0.20	44.000	165.750	166.375	0.036262554	2
11	1170	1300	140	0.15	32.375	214.500	217.750	0.021409895	2
12	1170	1400	160	0.10	17.625	167.250	188.000	0.031803581	4
13	1350	1100	200	0.15	23.000	202.000	167.500	0.029555194	3
14	1350	1200	180	0.10	20.375	176.500	143.875	0.039379478	4
15	1350	1300	160	0.25	44.125	265.500	225.250	0.016721324	1
16	1350	1400	140	0.20	69.667	285.000	348.625	0.010064602	2

the shallower the single cutting depth, related to the processing efficiency.

3 Simulation model

3.1 Geometric model and FE model

In order to deeply analyze the mechanism of laser processing CFRP, the 3D model of laser processing CFRP was established by finite element software, as shown in Fig. 4a. The geometry of the model is $380 \times 116 \times 35 \mu\text{m}$, the black-gray cylinders with a diameter of $10 \mu\text{m}$ represent carbon fiber tows, and the gray areas represent the resin matrix. Since both CFRP and heat source have symmetry, the symmetry plane is considered. The purpose is to reduce the computational cost without affecting the calculation results. The minimum mesh size of the FEM is $0.1 \mu\text{m}$. The process parameters of the simulation are the optimized and matched process parameters, as shown in bold values in Table 3.

3.2 Procedure and assumptions

The process of laser processing CFRP is very complex, involving many mechanisms, which makes the calculation of laser processing CFRP very difficult. Therefore, it will make reasonable assumptions to simplify the model in this paper:

- (1) Carbon fibers are evenly distributed in the resin matrix.
- (2) The influence of oxidation on the temperature rise process of the material is not considered.

- (3) When the temperature of carbon fiber and resin reaches the evaporative phase transition temperature, respectively, it is considered that this part of the material is removed.
- (4) The physical parameters of the material are constant and do not change with temperature.

In addition, when the material temperature rises to the evaporation phase transition temperature and is removed, the removed material no longer absorbs laser energy.

3.3 Governing equation and boundary conditions

In this study, we consider that all the laser energy absorbed by the material will be converted into heat. Therefore, the governing equation is only a time-dependent heat conduction equation. An implicit interface layer model was established to simulate the carbon fiber and resin interface. An interface layer material with no actual thickness was added between the resin matrix and the carbon fiber (the thickness of the representative geometric was set to $0.01 \mu\text{m}$). Romoli et al. [35] measured the laser absorption rate of epoxy resin. It was found that with the increase of laser wavelength, the absorptivity of epoxy resin on laser decreased gradually. When the laser wavelength is between 1000 and 1100 nm, the absorption rate of the resin is extremely low and can be ignored. In the FEM of this paper, the laser energy is only absorbed by the carbon fiber due to the laser wavelength used being 1064 nm. At the same time, the pulse width of the QCW fiber laser is at

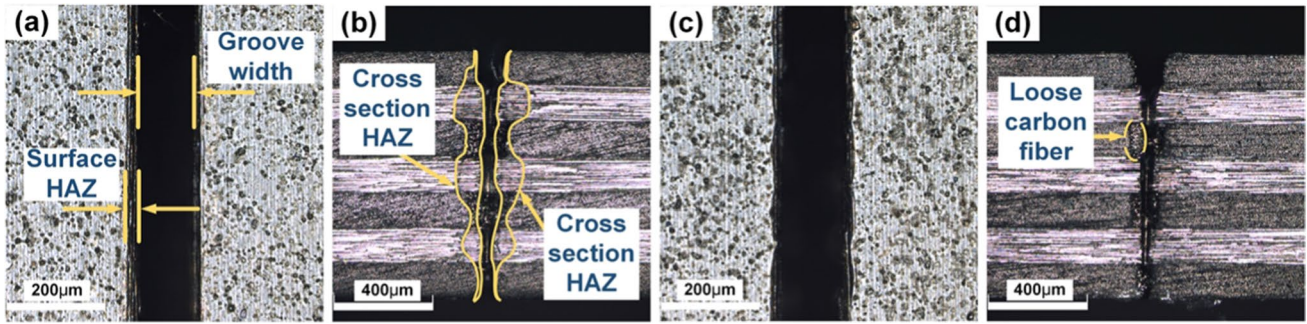


Fig. 3 The influence of different process parameters on machining quality. **a, b** The optimal group of the orthogonal experiment. **c, d** The optimal group of the range method

the millisecond level, which is much larger than the vibration time of the material lattice. Therefore, the classical heat conduction equation can be used to describe QCW fiber laser processing of CFRP [36]:

$$k_x \frac{\partial^2 T}{\partial t} + k_y \frac{\partial^2 T}{\partial t} + k_z \frac{\partial^2 T}{\partial t} + Q = \rho C \frac{\partial T}{\partial t} \tag{1}$$

where ρ is the density of the material, C is specific heat capacity of the material, Q is heat source (laser heat source in this paper), T is the temperature of a point (x, y, z) of the material, and $k_x, k_y,$ and k_z are the components of thermal conductivity k in $x-, y-$, and z -directions, respectively.

The pulsed laser mode is used to process CFRP, and the distribution in time can be described by the following equation:

$$g(t) = \begin{cases} 1, & t \leq \tau \\ 0, & t \geq \tau \end{cases} \tag{2}$$

where τ is pulse width of laser, 1 means the laser pulse is on, 0 means the laser pulse is off, and t is time in seconds.

Since laser processing mainly removes materials by thermal effect, the laser is equivalent to a heat source conforming to a Gaussian distribution in this paper, as shown

in Fig. 4b. The distribution of laser in time and space is as shown in Eq. (3):

$$q = (1 - R)\alpha_m \exp(\alpha_m z) \frac{2P_{\max}}{\pi r_b^2} \exp \frac{-2((x - V_0 t)^2 + (y - y_0)^2)}{r_b^2} g(t) \tag{3}$$

where q is the laser power density, P_{\max} is the peak laser power, V_0 is the moving speed of the center of the laser source along the x -axis, y_0 is the y -axis coordinate of the center of the laser source, r_b is the radius of laser, α_m is the absorption coefficient of the laser, and R is reflectivity of the material.

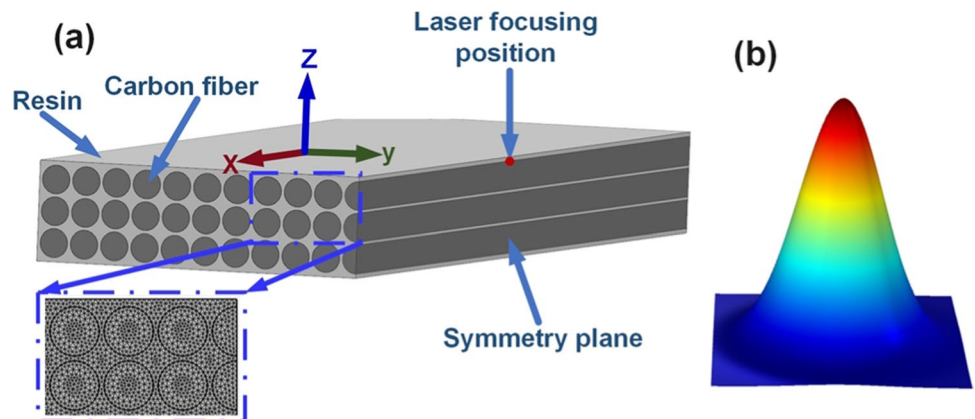
To ensure the uniqueness of the solution, the following boundary conditions need to be set, as shown in Eq. (4), (5), (6):

$$T(x, y, z, 0) = T_0 \tag{4}$$

$$k \frac{\partial T}{\partial n} = h_0(T - T_0) + \epsilon \sigma(T^4 - T_0^4) \tag{5}$$

$$\left(\lambda \frac{\partial T}{\partial n} \right)_I = \left(\lambda \frac{\partial T}{\partial n} \right)_{II}, T_I = T_{II} \tag{6}$$

Fig. 4 The model of finite element. **a** The model of finite element and the diagram of local mesh. **b** The model of Gaussian heat source



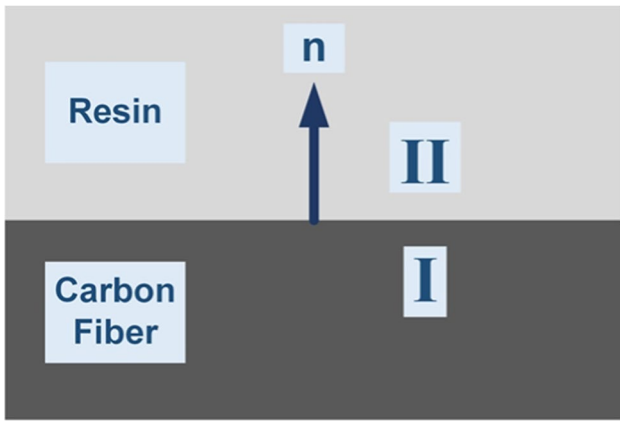


Fig. 5 The interfacial continuity conditions for heterogeneous materials

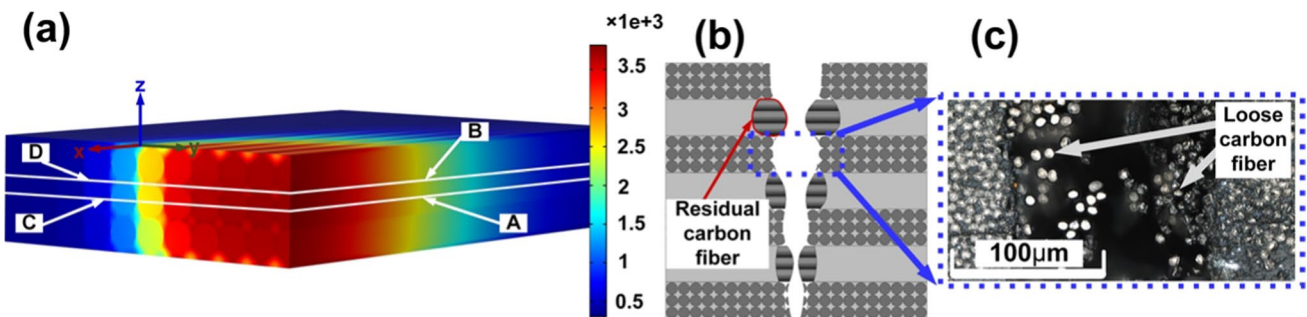


Fig. 6 The result of laser processing CFRP: (a) the temperature distribution characteristics of CFRP when the time is 0.1 ms; (b) the schematic diagram of CFRP removal section; (c) the loose image of carbon fiber

where T_0 is initial temperature, and its value is 300 K. h_o is convective heat transfer coefficient, ϵ is emissivity, σ is Stefan-Boltzmann constant, and its value is $5.67 \times 10^{-8} \text{ W}/(\text{m}^2 \cdot \text{K}^4)$. The laser irradiation surface is forced convection heat transfer, and the boundary conditions of other material surfaces are natural heat convection. Equation (6) is the interface continuity condition, as shown in Fig. 5.

4 Results and discussion

4.1 The temperature field behavior of laser ablation CFRP

When the laser irradiates the CFRP, the carbon fiber quickly absorbs the laser energy and excites the lattice vibration, and the laser energy is converted into heat energy. Finally, the temperature of the CFRP is increased to the evaporation phase transition temperature, as shown in Fig. 6a. Since this study only considers the absorption of laser energy by carbon fiber, the whole temperature of CFRP is determined by the energy absorbed by carbon

fiber. The temperature of the carbon fiber determines the temperature of the resin; that is, the temperature of the resin does not affect the maximum temperature of CFRP. Therefore, it is acceptable to continue increasing the temperature after the resin temperature reaches the temperature of the evaporative phase transition.

The cross-sectional temperature field distribution of laser processing CFRP is shown in Fig. 6a. In this study, the QCW fiber laser used is a Gaussian distribution in space, as shown in Fig. 4b. It can be seen that the temperature distribution range of the cross-section decreases from top to bottom, which is consistent with the processing characteristics of the cross-section in the experiment, which is wide at the top and narrow at the bottom, as shown in Fig. 7e and Fig. 8e. In order to explore the reasons for the formation of HAZ during laser processing,

the temperature distribution ranges of carbon fiber (line A in Fig. 6a) and resin (line B in Fig. 6a) in the x -axis direction at 0.1 ms were extracted. At the same time, the temperature distribution range diagram is shown in Fig. 9a. It can be seen from Table 1 that the latent heat of phase transition and evaporation temperature of resin are much lower than those of carbon fiber. The evaporative phase transition temperature of the resin is 698 K, and carbon fiber’s evaporative phase transition temperature is 3900 K. Therefore, the resin is easy to be removed during laser processing CFRP. When the temperature of the material exceeds the evaporative phase transition temperature, the material will be removed. It can be seen from Fig. 9a and b that the temperature of the resin has a larger range to reach the evaporative phase transition temperature. In comparison, the temperature of the carbon fiber has a smaller range to reach the evaporative phase transition temperature. This will lead to the phenomenon that a large amount of resin is removed and the carbon fibers are retained, as shown in Fig. 6b. Due to the inconsistent removal of carbon fiber and resin, HAZ will be formed,

as shown in Fig. 7 and Fig. 8. The carbon fibers become loose due to the lack of resin binding, as shown in Fig. 6c. As the carbon fiber becomes loose, the mechanical properties of CFRP are greatly reduced, which seriously affects the performance of CFRP, which is one of the factors that reduce the machining quality.

Since the FEM is symmetric about the x - z plane, the y -axis data was extracted to draw the temperature distribution range diagram of half the temperature distribution range of carbon fiber (line C in Fig. 6a) and resin (line D in Fig. 6a) at 0.1 ms, as shown in Fig. 9b. It can be seen from Fig. 9b that the maximum temperature of carbon fiber and resin gradually decreases as the distance from the center of the spot is farther. The resin temperature fluctuates near the center of the spot, as shown in Fig. 9b. This is because the carbon fiber is cylindrical, and the wave peak and wave valley positions are different from the carbon fiber, as shown in Fig. 9b. The wave peak is closer to the carbon fiber and can transfer more heat. Therefore, the temperature of the wave peak is higher. However, the distance between the wave valley and the carbon fiber is farther. Due to the small thermal conductivity of the resin, the heat conduction is limited when the distance is farther. Therefore, it is reasonable that the resin's temperature at the wave valley is lower than its temperature at the wave peak position. It can be seen from Fig. 9a and b that the temperature along the y -axis reaches the evaporation phase transition temperature of the carbon fiber which is larger than the x -axis. A larger groove width will be obtained when the cutting direction is parallel to the carbon fiber axis (the laser moves along the x -axis). This is because the radial thermal conductivity of carbon fiber is smaller than the axial thermal conductivity, which is more likely to cause heat accumulation and cause more material to be removed. This is consistent with the phenomenon of

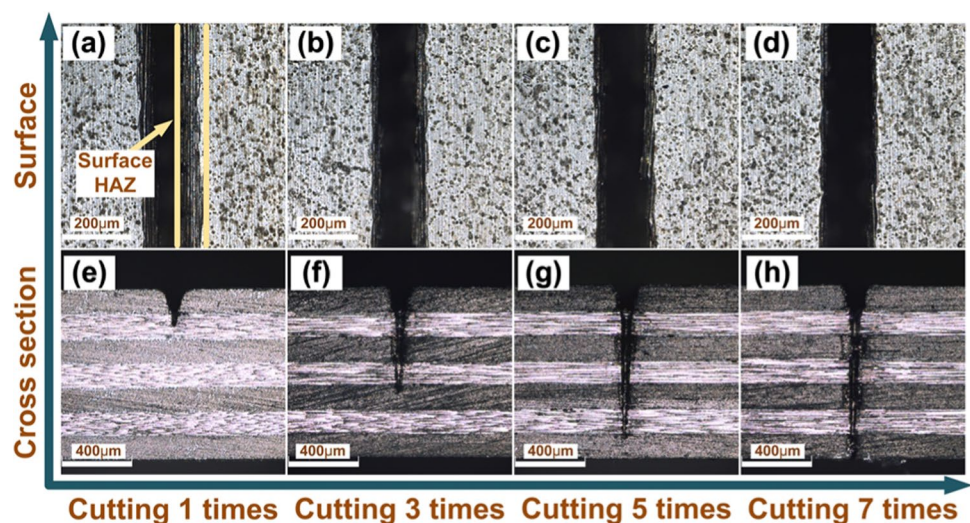
larger groove widths obtained when the cutting direction is parallel to the carbon fiber axis shown in Fig. 10b.

Similarly, the temperature range along the x -axis to the evaporative phase transition temperature of the resin is larger than the y -axis. A larger HAZ will be obtained when the cutting direction is perpendicular to the carbon fiber axis (the laser moves along the y -axis). It is because of the difference in the thermal conductivity of composite materials. Heat is more easily conducted along the carbon fiber axis, which will cause more resin to be removed, resulting in a larger HAZ. This is consistent with the phenomenon that the HAZ is larger when the cutting direction is perpendicular to the carbon fiber axis shown in Fig. 10a. As a result, it can be known from the simulation results that when the laser cutting direction is parallel to the carbon fiber axis, the thermal damage generated during the laser processing can be reduced.

Since the carbon fiber and the resin are in close contact, when the temperature of the carbon fiber increases, it will conduct heat energy to the resin, thereby causing the temperature of the resin to increase. For the thermal conductivity of inhomogeneous materials, different material regions satisfy the thermal conductivity differential equation, respectively. Since there is a step-change in the thermal conductivity of carbon fiber and resin, it is necessary to satisfy the continuity condition at the interface where the two materials are in contact, as shown in Eq. (6). Since the temperature of the resin is raised by the heat conduction of the carbon fiber, the maximum temperature of the resin is always lower than that of the carbon fiber during the processing, as shown in Fig. 9a and b.

$$\phi = \left(1 - \frac{v}{d \times f} \right) \times 100\% \quad (7)$$

Fig. 7 The effect of parallel carbon fiber axis to machining: **a–d** the surface machining quality; **e–h** the cross-section machining quality



where ϕ , v , d , and f are the spot overlap ratio, cutting speed, spot diameter, and laser frequency, respectively.

According to Eq. (7), by substituting the values in Table 3, it can be calculated that the light spots between two adjacent pulses do not overlap and have a certain distance. On the one hand, the heat accumulation can be reduced, and the machining efficiency can be improved due to the non-overlapping light spots. On the other hand, the non-overlapping of the light spots may reduce the processing quality, which is related to the cutting direction of the laser. When the cutting direction is parallel to the carbon fiber axis (the laser moves along the x -axis), the islands (part of the material that cannot be removed due to no laser irradiation) formed between the two pulses will have more resin removed under the rapid heat conduction of carbon fiber. It makes the mechanical properties of the islands severely reduced. At the same time, since the cutting direction is parallel to the axial processing of the carbon fiber, the carbon fiber in the island is incomplete and belongs to the broken carbon fiber, as shown in Fig. 11a. Therefore, the islands formed between the two pulses will be destroyed by the strong pressure shock of the material vapor and auxiliary gas. It will produce a large amount of fiber ablation debris, as shown in Fig. 12a. This will form a continuous, smooth kerf, as shown in experimental Fig. 7a–d. Therefore, the machining quality and machining efficiency are improved. However, when the cutting direction is perpendicular to the carbon fiber axis (the laser moves along the y -axis), less resin is removed from the islands formed between the two pulses, and good mechanical properties are retained. At the same time, due to the particularity of the processing direction, the carbon fibers in the islands are not completely broken, and only a small part of the carbon fibers on the surface are completely cut off under the heat accumulation, as shown in Fig. 11b. Therefore, the island cannot be completely destroyed under the action of material vapor and auxiliary gas. Therefore, no obvious fiber ablation debris will be produced during processing, as shown in Fig. 12b. This will result in a discontinuous kerf, which appears to be jagged, and the machining quality is reduced, as shown in experimental processing Fig. 7a–d.

The temperature field model shows that both the resin and the carbon fiber reach the evaporative phase transition temperature under the action of a single pulse, as shown in Fig. 9a and b. Meanwhile, the temperature of CFRP remains at phase transition temperature until the end of the pulse width. It means that the QCW fiber laser can achieve material removal with a single pulse. Surprisingly, it is consistent with the phenomenon that a single pulse can cause pulsed holes and achieve material removal when the cutting time is 1, as shown in Fig. 8a. Consequently, the conclusion obtained from the above temperature field model is consistent with the actual machining phenomenon. Based on the above analysis, it can be seen that the FEM

established in this paper can qualitatively reflect the response behavior of QCW fiber laser processing CFRP.

4.2 The results of ANOVA and main effect

In order to better evaluate the machining quality, it introduces a new parameter for evaluating the machining quality in this study, named the depth-heat-width ratio α .

$$\alpha = \frac{l}{d \times h} \quad (8)$$

where l , d , and h are groove depth, groove width, and the cross-section HAZ maximum, respectively.

It can be seen that Eq. (8) introduces the heat-affected zone factor based on aspect ratio. As we all know, the larger the aspect ratio, the better the machining quality. As for the machining quality, the smaller the value of the HAZ, the better the machining quality. The α is in the denominator. Therefore, the larger the α value, the better the machining quality. The cutting times are studied when analyzing the main effect in this paper. Since the multi-pass strategy is used to experiment in this study, the cutting times also represent the groove depth of a single cutting. The fewer the cutting times, the greater the single cutting depth and the higher the machining efficiency. It reflects the higher machining efficiency.

The statistical analysis demonstrated that a certain control factor of the experiment is significant at a confidence level of 95% (P -value < 0.05). The significant controls for machining quality in Table 6 are shown in bold. It can be seen from the machining quality evaluation indicators considered in this study that the laser power has a significant effect on the groove width but has no significant effect on other quality evaluation indicators. Cutting speed and laser frequency had no significant effect on all quality evaluation indicators. The laser pulse width significantly affects the groove width and the cutting times, but it has no significant effect on the HAZ and depth-heat-width ratio. The conclusions of this paper are closely related to the range of process parameters.

Simultaneously, the main effect of each process parameter on the machining quality was analyzed by the range method, as shown in Fig. 13. The abscissa is the process factor, and the ordinate is the machining quality evaluation indicator. In Fig. 13a, it can be concluded that the influence of various process factors on the surface HAZ is ranked as follows: pulse width $>$ laser power $>$ cutting speed $>$ laser frequency. In Fig. 13b, it can be concluded that the influence of various process factors on the groove width is ranked as follows: laser power $>$ pulse width $>$ laser frequency $>$ cutting speed. In Fig. 13c, it can be concluded that the influence of various process factors on the cross-section HAZ is ranked as follows: pulse

Table 6 ANOVA results for surface HAZ, groove width, cross-section HAZ, cutting times, and depth-heat-width ratio

Response factor	Control factor	DF	Adj SS	Adj MS	F-value	P-value	R-squared
Surface HAZ	Laser power (W)	3	520.174	173.391	2.206	0.266	0.922
	Laser frequency (Hz)	3	78.534	26.178	0.333	0.805	
	Cutting speed (mm/s)	3	471.215	157.072	1.999	0.292	
	Pulse width (ms)	3	1719.927	573.309	7.295	0.068	
	Residual	3	235.772	78.591			
	Total	15	19,701.600				
Groove width	Laser power (W)	3	11,947.512	3982.504	19.663	0.018	0.979
	Laser frequency (Hz)	3	3153.605	1051.202	5.190	0.105	
	Cutting speed (mm/s)	3	2017.230	672.410	3.320	0.175	
	Pulse width (ms)	3	10,737.980	3579.327	17.673	0.021	
	Residual	3	607.605	202.535			
	Total	15	604,450.063				
Cross section HAZ	Laser power (W)	3	3012.597	1004.199	0.887	0.538	0.924
	Laser frequency (Hz)	3	13,490.558	4496.853	3.971	0.144	
	Cutting speed (mm/s)	3	7282.370	2427.457	2.144	0.274	
	Pulse width (ms)	3	17,689.940	5896.647	5.208	0.104	
	Residual	3	3396.995	1132.332			
	Total	15	682,225.203				
Cutting times	Laser power (W)	3	2.750	0.917	3.667	0.157	0.971
	Laser frequency (Hz)	3	0.750	0.250	1.000	0.500	
	Cutting speed (mm/s)	3	0.750	0.250	1.000	0.500	
	Pulse width (ms)	3	20.750	6.917	27.667	0.011	
	Residual	3	0.750	0.250			
	Total	15	158.000				
Depth heat width ratio	Laser power (W)	3	0.001	0.000	1.800	0.321	0.901
	Laser frequency (Hz)	3	0.001	0.000	1.942	0.300	
	Cutting speed (mm/s)	3	8.983E-5	2.994E-5	0.229	0.871	
	Pulse width (ms)	3	0.002	0.001	5.164	0.105	
	Residual	3	0.000	0.000			
	Total	15	0.020				

The bold entries are the control factor has a significant impact on response factor

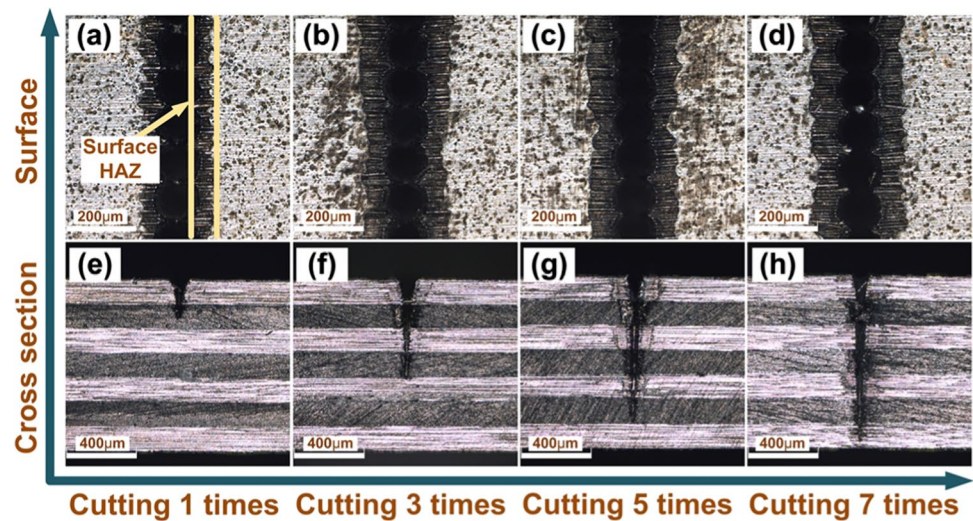
width > laser frequency > cutting speed > laser power. In Fig. 13d, it can be concluded that the influence of various process factors on the cutting times (the cutting times reflects the depth of the single cut) is ranked as follows: pulse width > laser power > cutting speed = laser frequency. In Fig. 13e, it can be concluded that the influence of various process factors on the depth heat width ratio is ranked as follows: pulse width > laser frequency > laser power > cutting speed. These conclusions are consistent with that of the analysis of variance.

From the ranking of the main effect of each process parameter on the machining quality, it can be seen that the influence of pulse width on each quality factor is the most important. This may be related to the interaction time between the laser and the material. Because the larger the pulse width, the more time the laser interacts with the material. Therefore, the cooling time is reduced, and it is

easy to cause heat accumulation of the material, resulting in greater thermal damage. In the evaluation indicators of machining quality, the smaller surface HAZ, cross-section HAZ, the groove width, and the larger the depth-heat-width ratio, the better the machining quality. The fewer cutting times, the higher the machining efficiency. According to the changing trend of the main effect graph in Fig. 13, the smaller the pulse width, the better the machining quality can be obtained. Without considering the machining efficiency, better machining quality can be obtained by shorter pulse width, lower power, higher cutting speed, and lower frequency. Since the depth-heat-width ratio can reflect the machining quality more comprehensively, the study mainly discusses the influence of process parameters on the depth-heat-width ratio.

It can be seen from Fig. 13e that the α value gradually increases as the laser power, laser frequency, and pulse width

Fig. 8 The effect of perpendicular carbon fiber axis to machining: **a–d** the surface machining quality; **e–h** the cross-section machining quality



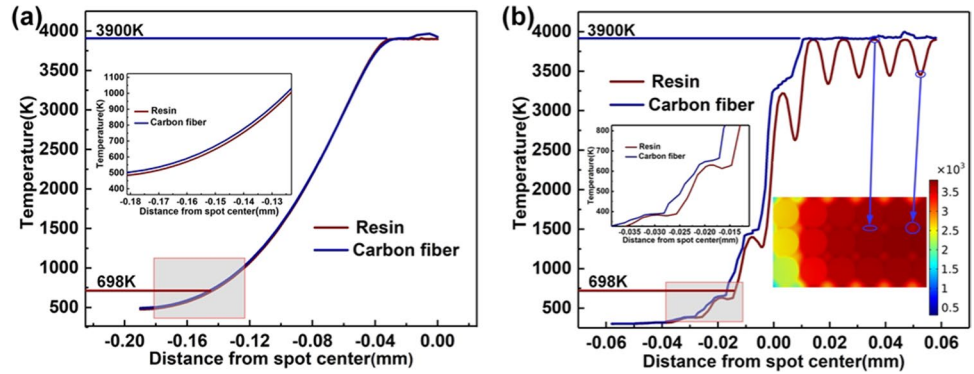
decrease. It means that the machining quality gradually increases with the decrease of the three process parameters. This is because reducing the three process parameters can reduce the laser energy absorbed by the material per unit of time. The cutting speed shows a trend of decreasing first and then increasing, showing a maximum value when the speed is 200 mm/s. The reason may be based on the cut penetration in this study. The depths of all orthogonal experimental groups are consistent. Therefore, the α value is determined by the groove width and the cross-section HAZ. It can be known from Eq. (8) that the α value is the reciprocal of the product of the groove width and the cross-section HAZ, and the larger the α value, the better the machining quality. According to Fig. 13e, it can be seen that the optimal process parameter combination when only considering the α -value is as follows: the pulse width, laser frequency, laser power, and cutting speed are 0.1 ms, 1100 Hz, 810 W, and 200 mm/s, respectively. However, the optimal level combination in the sixteen groups of orthogonal experiments is as follows: the pulse width, laser frequency, laser power, and cutting speed are 0.1 ms, 1100 Hz, 810 W, and 140 mm/s, respectively. There is only a speed difference with the optimal combination obtained by the range method. When the cutting speed is lower, the interaction time between the laser and the material is longer. The material absorbs more laser energy, so the number of cutting repetitions becomes less, but it will increase the residual heat of processing, and a larger HAZ is formed. When the cutting speed is higher, the interaction time between the laser and the material is shorter, and the laser energy absorbed by the material is less. Therefore, the residual heat of processing is reduced, and a smaller heat-affected zone is formed. Consequently, the HAZ generated during processing can be effectively reduced by using high-cutting speed processing. However, the cutting times increase as the cutting speed increases, which will cause the

CFRP to absorb energy repeatedly, and the groove width is increased. Therefore, when the speed increases, the α value first decreases and increases.

In this study, the machining quality of CFRP with a thickness of 1 mm was compared between the optimal experimental group and the optimal group of the range method. The experimental results show that compared with the optimal experimental group, the optimal group of the range method is as follows: The cutting times increased by up to 1, the groove width increased by up to 5.28%, the cross-section HAZ decreased by up to 7.88%, and α value increased by up to 3.11%. The experimental effect is shown in Fig. 3a–d. The surface HAZ of the optimal experimental group was 19.5 μm . Since the α value is mainly considered in this study, the following experiments are carried out using the optimal group of the range method (the pulse width, laser frequency, laser power, and cutting speed are 0.1 ms, 1100 Hz, 810 W, and 200 mm/s, respectively). When the cutting speed increases, since the laser energy absorbed by the material is reduced, the cutting times will be increased to achieve the material being cut through. This will cause the surface material to absorb laser energy multiple times, and the material removal and the groove width are increased. The inside of the kerf is effectively cooled, and the residual heat of processing is reduced. Consequently, the cross-section HAZ is reduced. Since the reduction of the cross-section HAZ is greater than the increase of the groove width, the α value increases. A better machining quality can be obtained by increasing the cutting speed.

It can be seen from Fig. 3a and c that the cutting kerf of the optimal experimental group is smoother than that of the optimal group of the range method. This is because the optimal experimental group and the optimal group of the range method are only different in speed. When the cutting speed increases and the laser frequency remains the same, the spot overlap rate will decrease, reducing the smoothness of the cutting kerf.

Fig. 9 The temperature distribution range of different directions: **a** the temperature distribution of *x*-axis; **b** the temperature distribution of *y*-axis



In order to estimate the influence of laser parameters on processing quality, the expression between input parameters and output parameters can generally be deduced through regression analysis. This paper conducted second-order polynomial regression analysis for the nonlinear relationship between process parameters and machining quality. In regression analysis, the response function is designed for all input variables and residuals, as described in Eq. 9.

$$y = f(x_{1u}, x_{2u}, x_{3u}, \dots, x_{iu}) + e_r \tag{9}$$

where $u(1,2,3,\dots,n)$ represents n observations in the experiment. The x_{iu} represents the level of the i th factors in u th observations. The response function is denoted by f and e_r is the residual.

In general, a second-order polynomial regression model for the output variable can be represented by the following.

$$A = \phi_0 + \sum_{i=1}^k \phi_i X_i + \sum_{i=1}^k \phi_{ii} X_i^2 + \sum_{i < j} \phi_{ij} X_i X_j + \epsilon_i \tag{10}$$

K represents the total number of factors (4 factors in this paper). The ϕ_0 is the intercept coefficient. The ϕ_i , ϕ_{ii} , and ϕ_{ij} stands for linear, quadratic, and interactive interactions, respectively.

In this paper, the regression equations of groove width, cross-section HAZ, and depth to heat-to-width ratio and process parameters can be expressed:

$$G_w = \alpha_0 + \alpha_1 \times P_{max} + \alpha_2 \times f + \alpha_3 \times V + \alpha_4 \times \tau + \alpha_5 \times P_{max}^2 + \alpha_6 \times f^2 + \alpha_7 \times V^2 + \alpha_8 \times \tau^2 + \alpha_9 \times P_{max} \times f + \alpha_{10} \times P_{max} \times V + \alpha_{11} \times P_{max} \times \tau + \alpha_{12} \times f \times V + \alpha_{13} \times f \times \tau + \alpha_{14} \times V \times \tau \tag{11}$$

$$\begin{aligned} HAZ_C = & \beta_0 + \beta_1 \times P_{max} + \beta_2 \times f + \beta_3 \times V \\ & + \beta_4 \times \tau + \beta_5 \times P_{max}^2 + \beta_6 \times f^2 + \beta_7 \times V^2 + \beta_8 \times \tau^2 \\ & + \beta_9 \times P_{max} \times f + \beta_{10} \times P_{max} \times V \\ & + \beta_{11} \times P_{max} \times \tau + \beta_{12} \times f \times V \\ & + \beta_{13} \times f \times \tau + \beta_{14} \times V \times \tau \end{aligned} \tag{12}$$

$$\begin{aligned} D_{h_w} = & \gamma_0 + \gamma_1 \times P_{max} + \gamma_2 \times f \\ & + \gamma_3 \times V + \gamma_4 \times \tau + \gamma_5 \times P_{max}^2 \\ & + \gamma_6 \times f^2 + \gamma_7 \times V^2 + \gamma_8 \times \tau^2 \\ & + \gamma_9 \times P_{max} \times f + \gamma_{10} \times P_{max} \times V \\ & + \gamma_{11} \times P_{max} \times \tau + \gamma_{12} \times f \times V \\ & + \gamma_{13} \times f \times \tau + \gamma_{14} \times V \times \tau \end{aligned} \tag{13}$$

The data brought into Table 5 can be used to calculate the respective coefficient values, as shown in Table 7.

It can be seen from Fig. 14 that the regression model is in good agreement with the experimental data. In the regression equation, R^2 for groove width, cross-section HAZ, and depth to heat-to-width ratio are 0.999, 0.962, and 0.993, respectively. It shows that the regression model established in this paper has high accuracy.

4.3 The influence of multiple cutting in different cutting directions on machining quality

In this study, the optimal group of the range method is used to compare the influence of cutting times and cutting direction on the machining quality, as shown in Fig. 10. The cutting direction refers to the included angle between the laser cutting direction and the axial direction of the first layer of carbon fiber. When the included angle is 0° , the laser cutting direction is parallel to the axial direction of the first layer of carbon fibers. On the contrary, when the included angle is 90° , the laser cutting direction is perpendicular to the axis of the first layer of carbon fibers. When the laser cutting direction is parallel to the axial direction of the carbon fiber, it

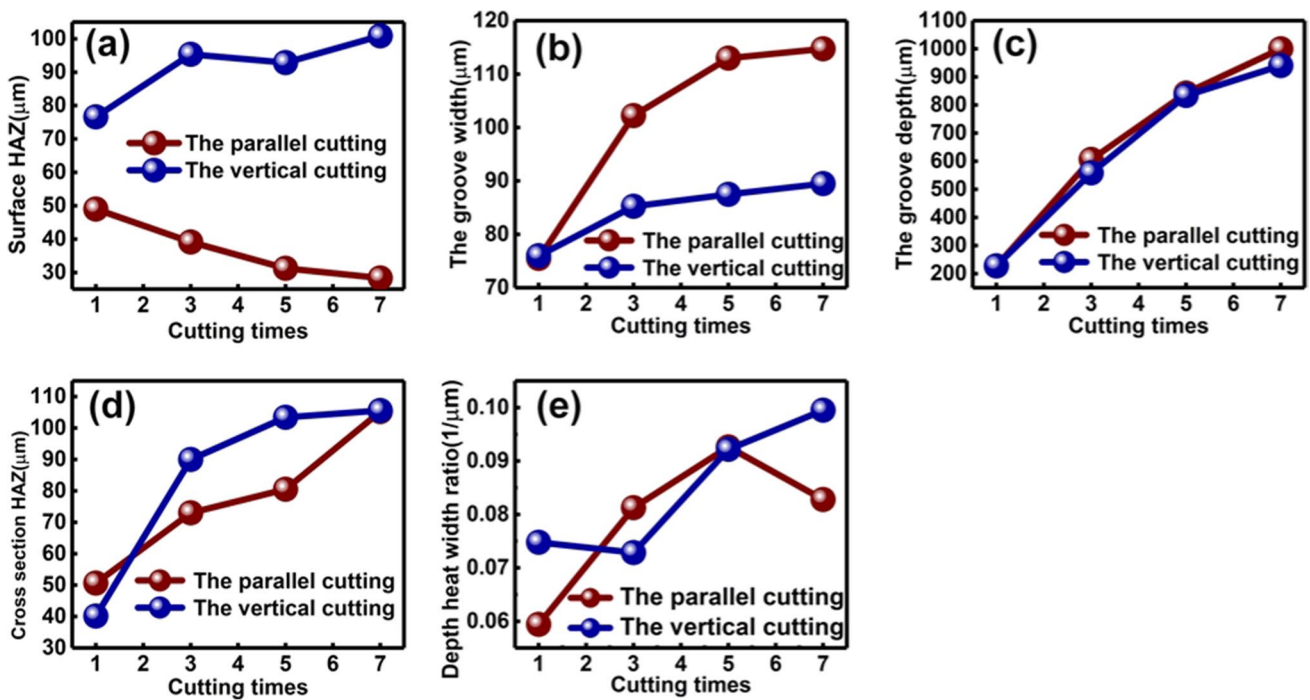


Fig. 10 The influence regular of cutting times on machining quality: **a** the surface HAZ; **b** the groove width; **c** the groove depth; **d** the cross-section HAZ; **e** the depth-heat-width ratio

to the simulation results in Section 4.1, when the laser cutting direction is parallel to the carbon fiber axial processing, it can be seen that the resin removal amount will be greater than the carbon fiber removal amount, resulting in the formation of HAZ and the exposed carbon fiber. As the number of cuts increases, the exposed carbon fibers repeatedly absorb the laser energy to form heat accumulation and are removed. As a result, as the number of cuts increases,

only takes seven times to cut through the CFRP. Therefore, the maximum cutting times is seven in this paper.

Figure 10a and b shows that as the cutting times increases, a smaller surface HAZ and a larger groove width can be obtained by the laser cutting direction parallel to the carbon fiber axis. This may be related to the fact that the laser has a Gaussian distribution in space; that is, the farther away from the center of the spot, the lower the energy. According

Table 7 Values of the coefficients of the regression equation

Factors	Value	Factors	Value	Factors	Value
α_0	-7,127,331.48830607	β_0	6,306,091.97469257	γ_0	-19,927.176337692
α_1	4065.63856502319	β_1	-3596.89804488975	γ_1	11.3658697176146
α_2	1920.2329489058	β_2	-1700.4227661706	γ_2	5.36885329651206
α_3	66,547.2233200787	β_3	-58,874.3050851043	γ_3	186.075419009859
α_4	-19,597,920.539415	β_4	17,345,905.6135629	γ_4	-54,806.6902407389
α_5	-1.99234199911752	β_5	1.76331858933811	γ_5	-0.00557175275695106
α_6	0.331451016271244	β_6	-0.291777401613402	γ_6	9.25736311886384E-4
α_7	-82.7612360204151	β_7	73.249820921449	γ_7	-0.231437992298991
α_8	11,917,355.8439375	β_8	-10,547,692.9181876	γ_8	33,328.5749925402
α_9	-0.000688362654578385	β_9	5.54461251607064E-6	γ_9	3.09569318694377E-7
α_{10}	-0.0024921879729186	β_{10}	-0.00170254423417485	γ_{10}	5.4716137635804E-7
α_{11}	0.583628065832223	β_{11}	-0.308244499789536	γ_{11}	9.07953403839581E-5
α_{12}	-29.7973119042851	β_{12}	26.3573095276069	γ_{12}	-0.0833175824045581
α_{13}	13,242.728779262	β_{13}	-11,718.2447128028	γ_{13}	37.0309649488496
α_{14}	-6628.61473853685	β_{14}	5849.59859867775	γ_{14}	-18.5132919097541

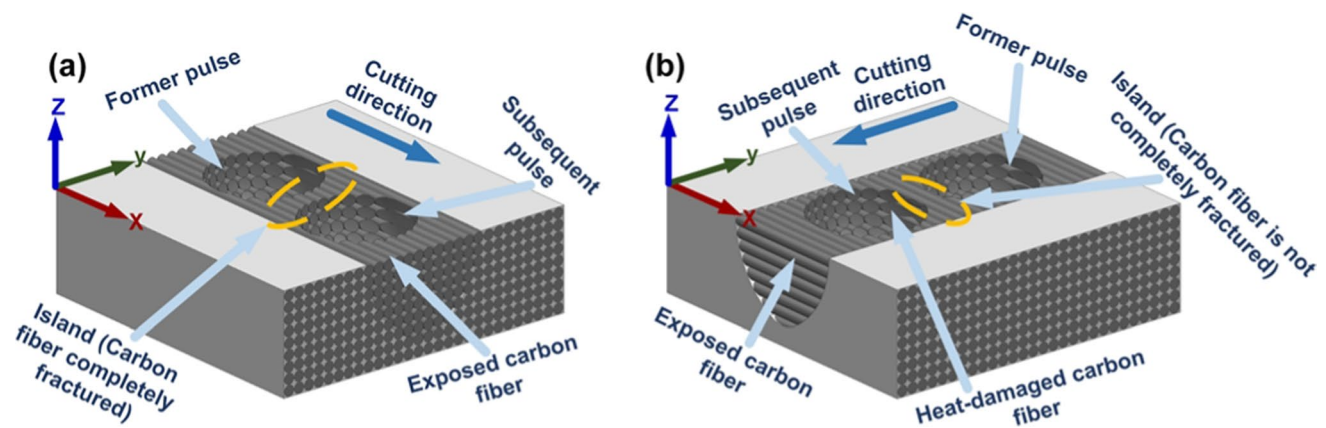
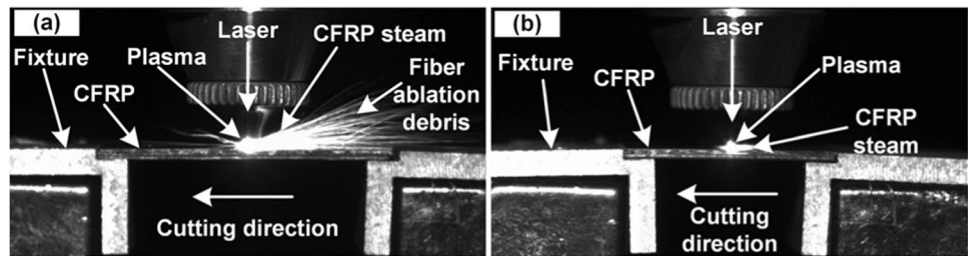


Fig. 11 The schematic diagram of island removal formed by different cutting directions. **a** The parallel carbon fiber axial machining. **b** The perpendicular carbon fiber axial machining

Fig. 12 The effect of cutting direction on the machining process: **a** the parallel the carbon fiber axis to machining; **b** the perpendicular the carbon fiber axis to machining



the groove width keeps increasing. At the same time, the scattered material on the edge of the groove is gradually removed, which will make the kerf smoother. However, the radial thermal conductivity of carbon fibers is small, and the heat transfer range is limited. The surface HAZ generated during processing is limited, and the increased groove width indicates that more carbon fibers are removed. Accordingly, a multi-pass strategy can reduce the surface HAZ when the laser cutting direction is parallel to the carbon fiber axis.

In contrast, when the laser cutting direction is perpendicular to the carbon fiber axis, the surface HAZ gradually increases, but the increase in the groove width is small. As the cutting times increase, the CFRP repeatedly absorbs the laser energy, resulting in more material being removed. Inversely, the axial thermal conductivity of carbon fiber is greater than the radial thermal conductivity. When the laser cutting direction is perpendicular to the carbon fiber axis, more laser energy will be transferred to the resin around the processing area, resulting in more resin being removed. Therefore, the surface HAZ is larger. This phenomenon is consistent with the simulation in Sect. 4.1, showing that resin removal temperature ranges larger when the laser cutting direction is perpendicular to the carbon fiber axis. With the increase in cutting times, more resin will be removed from the surface under the rapid thermal conductivity of carbon fiber, so the surface HAZ continues to increase. Due

to the insufficient energy of the irradiated laser edge for the groove width, less heat accumulation is formed under the effect of rapid thermal conduction of the carbon fiber. Accordingly, as the cutting times increase, the amount of carbon fiber removed gradually decreases, and the increase in groove width is smaller, as shown in Fig. 10b.

It can be seen from Fig. 10c and d that both machining directions show that with the increase in cutting times, the groove width and the cross-section HAZ gradually increase. This is related to the abovementioned repeated absorption of laser energy by CFRP. With the increase in cutting times, the material inside the slit continuously absorbs the laser energy, increasing heat accumulation so that more material reaches the removal temperature and is removed. Therefore, the groove depth continues to increase. However, the laser focus is focused on the CFRP surface. As the groove depth increases, the laser energy absorbed by the material inside the slit will gradually decrease, decreasing the amount of material removed during each cut. Therefore, the increase in the groove depth tends to decrease. Unfortunately, the cooling effect of the assist gas is limited as the groove depth increases. When the material inside the slit repeatedly absorbs the laser energy, heat accumulation will be formed inside the slit, causing more resin to be removed under the rapid heat conduction of the carbon fiber. Therefore, as the increase of cutting times, the cross-section HAZ will continue to increase. When the laser

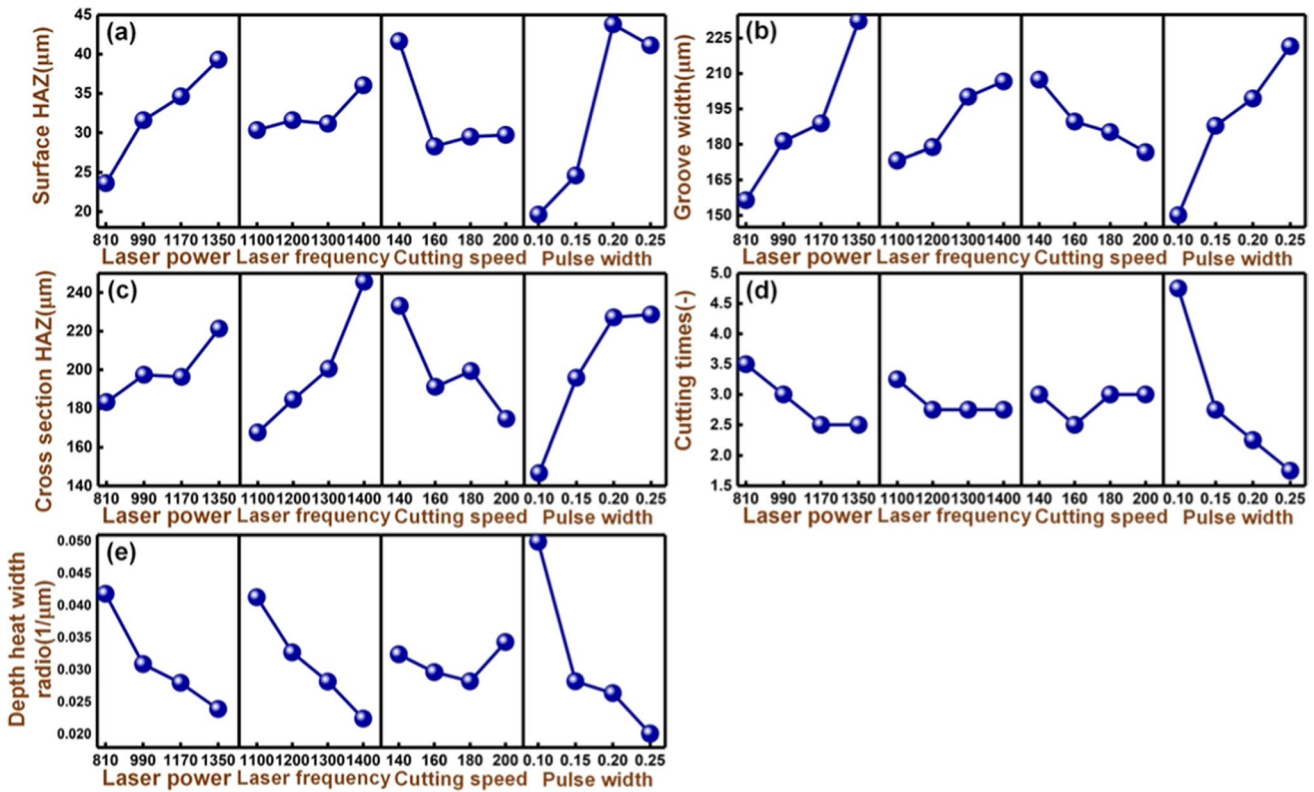


Fig. 13 The range results. a Surface HAZ. b Groove width. c Cross-section HAZ. d Cutting times. e Depth-heat-width ratio

cutting direction is parallel to the axial direction of the carbon fiber, the groove width can be larger, which enhances the cooling effect inside the slit. Consequently, a multiple-pass strategy can obtain a smaller cross-section HAZ when the laser cutting direction is parallel to the carbon fiber axis.

Figure 10e shows the regular variation of α under different cutting times and machining directions. The α is determined by the groove depth, width, and cross-section HAZ. When the cutting times is one, the α value is larger by the laser cutting direction perpendicular to the carbon fiber axis, indicating better machining quality. This is related to the larger cross-section HAZ formed by laser processing parallel to the carbon fiber axis when the cutting times is one. It can be seen from Fig. 10c that when the cutting times is one, the groove depth can reach the second layer of CFRP. It can be seen from Fig. 1 that compared with the laser processing perpendicular to the carbon fiber axis, when the laser cutting direction is parallel to the carbon fiber axis, the thermal conductivity of the second layer along the two sides of the slit is greater. Therefore, more heat will be transferred to both sides of the kerf, causing more resin to be removed, resulting in a larger cross-sectional HAZ. When the cutting times are seven, the α value is larger when the laser cutting direction is perpendicular to the carbon fiber axis. This is mainly related to the size of the groove width, and

the other indicators are almost the same. Therefore, when the cutting times are one and seven, the laser cutting direction is perpendicular to the carbon fiber axial direction that can obtain better machining quality. A larger α value can be obtained when the laser cutting direction is parallel to the carbon fiber axis when the cutting times are three. This is mainly related to the smaller cross-sectional HAZ obtained by the laser cutting direction parallel to the carbon fiber axis. When the cutting times are five, the machining quality of the two processing directions is almost identical. This is because α is jointly determined by the groove width, depth, and cross-section HAZ caused by multiple factors Fig. 7.

Consequently, compared with the thermal damage produced by literature [17], the minimum cross-section HAZ produced by laser cutting is 105 μm when the cutting speed used is as high as 200 mm/s in this study, which is reduced by 38%. Although literature [16] has different ways of characterizing HAZ, the scale bar can calculate the approximate surface HAZ range. By comparison, it can be known that the pulse mode processing in this study can significantly reduce the HAZ. Homoplasticly, compared with the reference [34] that uses QCW fiber laser to process CFRP with high power and produces a cross-section HAZ of 500 μm , the processing method adopted in this paper reduces the HAZ by up to 79% to the greatest extent.

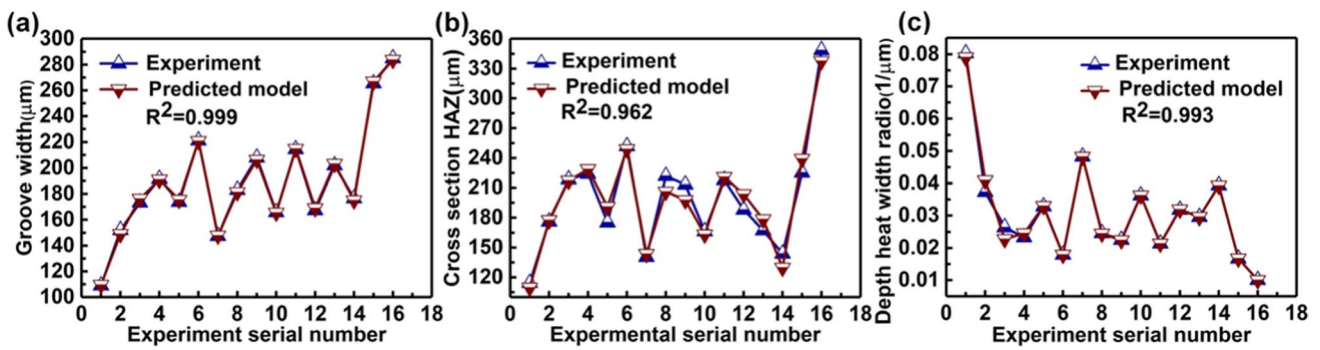


Fig. 14 Comparison of machining quality between the experimental date and the predicted model: **a** groove width; **b** cross-section HAZ; **c** deep heat width ratio

Consequently, the thermal damage can be effectively reduced by the processing method in this paper (Fig. 8).

4.4 The analysis of removal mechanism of multi-pass cutting CFRP by QCW fiber laser

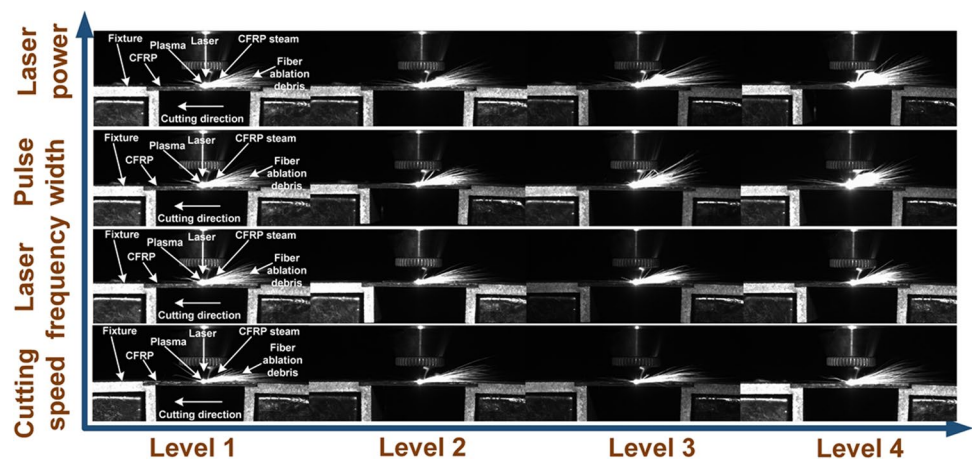
$$E = \frac{p_{\max} \times \tau}{\pi \times r_0^2} \tag{14}$$

where I , p_{\max} , r_0 , and τ are laser energy density, peak power, spot radius, and pulse width, respectively.

Ma et al. [37] used the shadow method to photograph the plasma generated during millisecond laser processing of CFRP and GFRP by a high-speed camera. The results show that there will be plasma generation when the energy density exceeds $392(\text{J}/\text{cm}^2)$. According to Eq. (14), the laser energy density in this paper can be calculated. There will be plasma generation during the laser processing CFRP due to the minimum energy density in this paper being $1031(\text{J}/\text{cm}^2)$. The residues produced are sprayed out of the slit by processing under the action of the plasma shock wave. It is beneficial in promoting the interaction between the laser and the material. Figure 15

shows that based on the laser power, laser frequency, cutting speed, and pulse width are 810 W, 1100 Hz, 200 mm/s, and 0.1 ms, respectively, according to the process parameters given in Table 3 to in situ capture the processing process by a high-speed camera PCO. dimax HD. It can be seen from Fig. 8 that there is obvious CFRP steam and fiber ablation debris during the laser processing. There is a small amount of black matter attached to the surface of CFRP, which is the product of the carbonization of the material at high temperatures. At the same time, there is a small amount of smoke during the laser processing process. The plasma and smoke will cause laser loss and reduce machining efficiency. However, the coaxial gas method is beneficial for accelerating the escape of plasma and smoke from the processing area and weakening its influence on the laser transmission. The simulation results in Sect. 4.1 show that the instantaneous temperature of the laser machining area can reach the phase transition removal temperature of carbon fibers under the action of a pulsed laser, which indicates that the carbon fibers are mainly removed by sublimation during pulsed laser processing [38]. During the heating process of the material, it will experience a very short liquid phase. The molten material will be removed by the impact of auxiliary

Fig. 15 The influence of different process parameters on the machining process



gas and plasma, but the process is very short. However, the thermoset epoxy resins are not considered to undergo a liquid phase. The removal of epoxy resins is mainly by pyrolysis and sublimation. Consequently, the removal of CFRP is mainly based on sublimation removal.

When high cutting speed and multi-pass strategy are used for laser processing, the laser energy absorbed by the material during a single cut is limited, only a small amount of material can be removed, and the cutting depth is shallow. Therefore, the study mainly realizes CFRP processing by layer-by-layer milling, as shown in Fig. 7 and Fig. 8. Due to the small amount of material removed by a single cut, the coaxial auxiliary gas is conducive to ejecting processing residues such as ablated fibers inside the slit, as shown in Fig. 15 and Fig. 12. At the same time, the auxiliary gas can effectively cool the kerf. On the one hand, this is beneficial to promote the interaction between the laser and the material in the next cutting. On the other hand, the ablative fibers are jetted out of the slit to prevent the ablative fibers from transferring heat inside the slit without removing material. Additionally, the auxiliary gas can reduce the heat accumulation inside the slit and avoid excessive thermal damage to the material. It can be seen from the previous analysis that a larger groove width can be obtained when the laser cutting direction is parallel to the carbon fiber axis, which will help the auxiliary gas to cool the inside of the slit effectively. As a result, a smaller HAZ can be obtained when the laser cutting direction is parallel to the carbon fiber axis, as shown in Fig. 10d.

According to Table 1, the removal threshold of resin is one order of magnitude lower than that of carbon fiber, so the resin is easier to be removed during laser processing. The simulation model established in this paper shows that the range of reaching the resin removal threshold is larger than the carbon fiber removal threshold during laser processing, as shown in Fig. 9a and b. There is a phenomenon that more resin will be removed, but the carbon fiber will remain, and the HAZ will be formed. Consequently, the formation of HAZ is due to inconsistent removal of carbon fiber and resin. Due to the lack of resin restraint, the mechanical properties of carbon fiber will be decreased. Under the impact of material vapor and auxiliary gas, the carbon fibers that have not been removed will become loose, as shown in Fig. 6c, and even the fiber pull-out phenomenon will occur.

Interestingly, when the laser cutting direction is parallel to the carbon fiber axis, the resin between the two pulses is quickly removed by heat conduction due to the fast thermal conductivity of the carbon fiber. And the residual carbon fiber belongs to the broken carbon fiber with extremely poor mechanical properties. Under the impact of high-pressure gas, the residual carbon fiber will be further removed by mechanical erosion, such as fiber ablation debris, as shown in Fig. 15, which is beneficial to making the slit smoother. On the contrary, when the laser cutting direction

is perpendicular to the carbon fiber axis, the mechanical properties of the residual carbon fiber between the two pulses are better. It cannot be completely removed under the impact of high-pressure gas, and the fiber ablation debris is not significant, as shown in Fig. 12b, so the slit is serrated. Accordingly, mechanical erosion during the laser processing of CFRP can improve the machining quality and efficiency.

The multi-pass strategy is achieved by removing material layer by layer. During the multi-pass strategy process, the material's temperature rises because the material inside the slit repeatedly absorbs the laser energy. The heat accumulation will form inside the kerf, rapidly conducting the heat through the carbon fiber, causing more resin to be removed. Still, the carbon fiber is difficult to remove. Therefore, as the cutting times increase, a larger HAZ will be generated in the cross-section, and the cross-section HAZ will gradually increase from 50 to 105 μm . Conversely, since the laser is focused on the material's surface, the surface material absorbs more laser energy than the inside of the slit. When the laser cutting direction is parallel to the carbon fiber axis, the groove width will increase with the cutting times, which is beneficial to reducing the surface HAZ. The surface HAZ gradually decreases from the initial 49 to 28 μm , as shown in Fig. 10a. When the laser cutting direction is perpendicular to the carbon fiber axis, with the increase in cutting times, the bare carbon fiber is removed repeatedly by absorbing energy, and the groove width is increased. Unfortunately, the carbon fiber will continuously transfer heat to the resin during the subsequent process. Therefore, as the cutting time increases, the surface HAZ increases from the initial 76 to 100 μm ; the cross-sectional HAZ increases from the initial 41 to 105 μm .

However, when machining with high power and long pulse width, the ablation debris, plasma concentration, and residual heat generated during machining increase rapidly, as shown in Fig. 15 for machining phenomena at different levels. At this time, the cooling effect of the auxiliary gas is limited, which will cause considerable thermal damage. The cross-sectional HAZ is 348.625 μm , and the surface HAZ is 69.667 μm . As a result, the thermal damage generated during the laser processing CFRP will be decreased using the pulsed mode, higher power, and multi-pass strategy.

5 Conclusions

The present work conducted the multi-pass strategy experiment of 450 W QCW fiber laser processing CFRP on CFRP by the DOE. And the effects of process parameters (laser power, laser frequency, pulse width, and cutting speed) on the machining were analyzed statistically. The HAZ formation mechanism and material removal mechanism of QCW pulsed laser processing CFRP were clarified by combining

the experimental study and finite element model. A method of effectively controlling thermal damage during QCW laser processing of CFRP was obtained. The main conclusions are as follows:

- (1) The material removal mechanisms of QCW fiber laser processing of CFRP mainly include thermal evaporation, thermal melting, plasma impact, mechanical ablation, pyrolysis, and carbonization. The mechanical ablation effect generated during laser processing can increase the material removal rate and improve processing quality and efficiency.
- (2) The characteristics of temperature field distribution show that, compared with the processing perpendicular to the carbon fiber axial direction, the temperature field distribution range is smaller when the laser cutting direction is parallel to the carbon fiber axial direction. Therefore, a smaller HAZ and a larger groove width can be obtained. Similarly, the thermal damage can be effectively controlled when the laser cutting direction is parallel to the carbon fiber axis with the increase in cutting times. The machining quality can be improved.
- (3) Experiments and simulations show that a pulsed laser can make the temperature of CFRP reach the material removal temperature to achieve material removal. At the same time, HAZ will be formed when the removal of carbon fiber and resin is inconsistent.
- (4) This paper uses the optimal process parameter group within the range of process parameters: the pulse width is 0.1 ms, the laser frequency is 1100 Hz, the laser power is 810 W, and the cutting speed is 200 mm/s.
- (5) Compared with previous studies, this paper proposes that high-speed and high-power processing in pulsed mode can enhance the cooling effect of the machining area and avoid excessive heat accumulation. The method can effectively control thermal damage during CFRP laser processing. The minimum surface HAZ is 19.5 μm .

Author contribution Liao Zhou: conceptualization, methodology, formal analysis, investigation, data curation, writing—original draft, writing—review and editing. Hui Jiao, Ping Huang, and Guanghui Zhang: conceptualization, validation, formal analysis, supervision, writing—review and editing. Ze Lin and Zhen Zhao: resources, data curation. Yuxing Huang, Jia Zhou, and Yuhong Long: supervision, writing—review and editing.

Funding This work was financially supported and funded by Guangxi Natural Science Foundation (2020JJB170048, 2019JJD160010), Guangxi Science and Technology Base and Talent Project (2021AC18026), the National Natural Science Foundation of China (NSFC) (62274045, 62004050, 52165056), Guangxi Key Laboratory of Manufacturing Systems and Advanced Manufacturing Technology

(17–259-05-018Z), Guangxi Young Teacher Education Project (2020KY05020), the Innovation Project of Guangxi Graduate Education (YCSW2022287, YCBZ2022114, YCBZ2021073), the GUET Excellent Graduate Thesis Program (19YJPYBS02), and the Innovation Project of GUET Graduate Education (2020YCX010, 2021YCX001).

Data availability The authors confirm that the data supporting the findings of this study are available within the article.

Declarations

Ethical approval Not applicable.

Consent to participate Not applicable.

Consent for publication Not applicable.

Conflict of interest The authors declare no competing interests.

References

1. Al-sammari AT, Brena SF (2021) Strength of carbon fiber-reinforced polymer (CFRP) sheets bonded to concrete with CFRP spike anchors. *ACI Struct J* 118(1):153–166. <https://doi.org/10.14359/51728084>
2. Liu Y, Xie J, Tafsirojjaman T, Yue Q, Tan C, Che G (2022) CFRP lamella stay-cable and its force measurement based on microwave radar. *Case Stud Construct Mater* 16:e00824. <https://doi.org/10.1016/j.cscm.2021.e00824>
3. Zheng H, Zhang W, Li B, Zhu J, Wang C, Song G, Wu G, Yang X, Huang Y, Ma L (2022) Recent advances of interphases in carbon fiber-reinforced polymer composites: a review. *Compos Part B:Eng* 233:109639.0. <https://doi.org/10.1016/j.compositesb.2022.109639>
4. Soutis C (2005) Fibre reinforced composites in aircraft construction. *Prog Aerosp Sci* 41(2):143–151. <https://doi.org/10.1016/j.paerosci.2005.02.004>
5. Kodama H, Okazaki S, Jiang Y, Yoden H, Ohashi K (2020) Thermal influence on surface layer of carbon fiber reinforced plastic (CFRP) in grinding. *Precis Eng* 65:53–63. <https://doi.org/10.1016/j.precisioneng.2020.04.005>
6. Colak O, Sunar T (2016) Cutting forces and 3D surface analysis of CFRP milling with PCD cutting tools. *Procedia CIRP* 45:75–78. <https://doi.org/10.1016/j.procir.2016.03.091>
7. Han La, Zhang J, Liu Y, Sun T (2021) Effect of fiber orientation on depth sensing intra-laminar failure of unidirectional CFRP under nano-scratching. *Compos B Eng* 224:109211. <https://doi.org/10.1016/j.compositesb.2021.109211>
8. Fuji W, Guangjian Bi, Fuda N (2021) Modeling of dynamic milling forces considering the interlaminar effect during milling multidirectional CFRP laminate. *J Reinf Plast Compos* 40(11–12):437–449. <https://doi.org/10.1177/0731684420971760>
9. Iqbal A, Zhao G, Zaini J, Jamil M, Napman MM, Khan AM, Zhao W, He N, Suhaimi H (2021) CFRP drilling under throttle and evaporative cryogenic cooling and micro-lubrication. *Compos Struct* 267:113916. <https://doi.org/10.1016/j.compstruct.2021.113916>
10. Habib S, Okada A (2016) Influence of electrical discharge machining parameters on cutting parameters of carbon fiber reinforced plastic. *Mach Sci Technol* 20(1):99–114. <https://doi.org/10.1080/10910344.2015.1133914>
11. Kurniawan R, Kumaran ST, Prabu VA, Zhen Y, Park KM, Kwak YI, Islam MM, Ko TJ (2017) Measurement of burr removal rate

- and analysis of machining parameters in ultrasonic assisted dry EDM (US-EDM) for deburring drilled holes in CFRP composite. *Measurement* 110:98–115. <https://doi.org/10.1016/j.measurement.2017.06.008>
12. Youssef HA, El-Hofy HA, Abdelaziz AM, El-Hofy MH (2021) Accuracy and surface quality of abrasive waterjet machined CFRP composites. *J Compos Mater* 55(12):1693–1703. <https://doi.org/10.1177/0021998320974428>
 13. Popan IA, Bocanet V, Balc N, Popan AI (2019) Investigation on feed rate influence on surface quality in abrasive water jet cutting of composite materials, monitoring acoustic emissions. *Adv Manuf Eng Mater* (103-105):105–113. https://doi.org/10.1007/978-3-319-99353-9_12
 14. Monoranu M, Ashworth S, M' Saoubi R, Fairclough JP, Kerrigan K, Scaife RJ, Barnes S, Ghadbeigi H (2019) A comparative study of the effects of milling and abrasive water jet cutting on flexural performance of CFRP. *Procedia CIRP*. 85:277–283. <https://doi.org/10.1016/j.procir.2019.09.036>
 15. Emmelmann C, Petersen M, Goeke A, Canisius M (2011) Analysis of laser ablation of CFRP by ultra-short laser pulses with short wavelength. *Phys Procedia* 12:565–571. <https://doi.org/10.1016/j.phpro.2011.03.071>
 16. Maojun Li, Shuo Li, Xujing Y, Yi Z, Zhichao L (2018) Fiber laser cutting of CFRP laminates with single- and multi-pass strategy: a feasibility study. *Opt Laser Technol* 107:443–453. <https://doi.org/10.1016/j.optlastec.2018.06.025>
 17. Leone C, Genna S (2018) Heat affected zone extension in pulsed Nd:YAG laser cutting of CFRP. *Compos B Eng* 140:174–182. <https://doi.org/10.1016/j.compositesb.2017.12.028>
 18. Maojun Li, Guocui G, Yi Z, Xujing Y (2020) Thermal defect characterization and strain distribution of CFRP laminate with open hole following fiber laser cutting process. *Opt Laser Technol* 122:105891. <https://doi.org/10.1016/j.optlastec.2019.105891>
 19. Viboon T, Ketsada K, Huan Qi (2019) Investigation into laser machining of carbon fiber reinforced plastic in a flowing water layer. *Int J Adv Manuf Technol* 104(9–12):3629–3645. <https://doi.org/10.1007/s00170-019-04131-0>
 20. Kaakkunen JJJ, Silvennoinen M, Paivasaari K, Vahimaa P (2011) Water-assisted femtosecond laser pulse ablation of high aspect ratio holes. *Phys Procedia* 12:89–93. <https://doi.org/10.1016/j.phpro.2011.03.110>
 21. Dong S, Fuzhu H, Weisheng Y (2019) The experimental investigation of water jet-guided laser cutting of CFRP. *Int J Adv Manuf Technol* 102(1–4):719–729. <https://doi.org/10.1007/s00170-018-03218-4>
 22. Dong S, Fuzhu H, Weisheng Y, Chaolong J (2018) Surface integrity of water jet guided laser machining of CFRP. *Procedia CIRP* 71:71–74. <https://doi.org/10.1016/j.procir.2018.05.073>
 23. Zhang Y, Qiao H, Zhao J, Cao Z, Yu Y (2020) Numerical simulation of water jet-guided laser micromachining of CFRP. *Mater Today Commun* 25:101456. <https://doi.org/10.1016/j.mtcomm.2020.101456>
 24. Yaowen Wu, Guangyi Z, Jianxin W, Yang C, Wenwu Z (2021) The cutting process and damage mechanism of large thickness CFRP based on water jet guided laser processing. *Opt Laser Technol* 141:107140. <https://doi.org/10.1016/j.optlastec.2021.107140>
 25. Staehr R, Bluemel S, Hansen P, Jaeschke P, Suttmann O, Overmeyer L (2015) The influence of moisture content on the heat affected zone and the resulting in-plane shear strength of laser cut thermoplastic CFRP. *Plast Rubber Compos* 44(3):111–116. <https://doi.org/10.1179/1743289814Y.0000000114>
 26. Riveiro A, Quintero F, Lusquiños F, Del Val J, Comesaña R, Boutinguiza M, Pou J (2017) Laser cutting of carbon fiber composite materials. *Procedia Manuf* 13:388–395. <https://doi.org/10.1016/j.promfg.2017.09.026>
 27. Yuji S, Masahiro T, Fumihiko M, Tomomasa O, Nobuyuki A (2017) Thermal effect on CFRP ablation with a 100-W class pulse fiber laser using a PCF amplifier. *Appl Surf Sci* 417:250–255. <https://doi.org/10.1016/j.apsusc.2017.03.286>
 28. Negarestani R, Li L, Sezer HK, Whitehead D, Methven J (2010) Nano-second pulsed DPSS Nd:YAG laser cutting of CFRP composites with mixed reactive and inert gases. *Int J Adv Manuf Technol* 49(5–8):553–566. <https://doi.org/10.1007/s00170-009-2431-y>
 29. Kononenko TV, Freitag C, Komlenok MS, Onuseit V, Weber R, Graf T, Konov VI (2014) Oxygen-assisted multipass cutting of carbon fiber reinforced plastics with ultra-short laser pulses. *J Appl Phys* 115(10):103107. <https://doi.org/10.1063/1.4868385>
 30. Dirk H, Peter J, Oliver M, Heinz H (2008) Investigations on the thermal effect caused by laser cutting with respect to static strength of CFRP. *Int J Mach Tools Manuf* 48(12–13):1464–1473. <https://doi.org/10.1016/j.ijmachtools.2008.04.007>
 31. Schneider F, Wolf N, Petring D (2013) High power laser cutting of fiber reinforced thermoplastic polymers with cw- and pulsed lasers. *Phys Procedia* 41:415–420. <https://doi.org/10.1016/j.phpro.2013.03.096>
 32. Maojun Li, Shuo Li, Guocui G, Yi Z, Zhichao L, Xujing Y (2019) Experimental study on hole quality and tensile progressive failure following fiber laser cutting of multidirectional carbon fiber reinforced plastic laminates. *J Laser Appl* 31(1):12004. <https://doi.org/10.2351/1.5046549>
 33. Dirk H, Matthias S-L, Marten C, Max O, Jan-Philipp T, Claus E (2015) Laser cutting of carbon fiber reinforced plastic using a 30kW fiber laser. *J Laser Appl* 27(S2):S28001. <https://doi.org/10.2351/1.4906304>
 34. Leone C, Mingione E, Genna S (2021) Laser cutting of CFRP by quasi-continuous wave (QCW) fibre laser: effect of process parameters and analysis of the HAZ index. *Compos B Eng* 224:109146. <https://doi.org/10.1016/j.compositesb.2021.109146>
 35. Romoli L, Fischer F, Kling R (2012) A study on UV laser drilling of PEEK reinforced with carbon fibers. *Opt Lasers Eng* 50(3):449–457. <https://doi.org/10.1016/j.optlaseng.2011.10.008>
 36. He Y, Hanxiang L, Rixiang G, Liu Xin Yu, Xi SF, Lisa L (2022) Numerical simulation of paint stripping on CFRP by pulsed laser. *Opt Laser Technol* 145:107450. <https://doi.org/10.1016/j.optlastec.2021.107450>
 37. Yao Ma, Chao X, Wei Z, Guangyong J (2021) Experimental study of plasma plume analysis of long pulse laser irradiates CFRP and GFRP composite materials. *Crystals* 11(5):545. <https://doi.org/10.3390/cryst11050545>
 38. Tao N, Chen G, Fan L, Wang B, Li M, Fang W (2021) Temperature-dependent material removal during pulsed laser processing of CFRP composites. *Opt Laser Technol* 144:107445. <https://doi.org/10.1016/j.optlastec.2021.107445>

Publisher's note Springer Nature remains neutral with regard to jurisdictional claims in published maps and institutional affiliations.

Springer Nature or its licensor (e.g. a society or other partner) holds exclusive rights to this article under a publishing agreement with the author(s) or other rightsholder(s); author self-archiving of the accepted manuscript version of this article is solely governed by the terms of such publishing agreement and applicable law.